Andreas Niedermeier · Danielle Hoja · Susanne Lehner

Topography and morphodynamics in the German Bight using SAR and optical remote sensing data

Abstract Morphological changes in coastal areas, especially in river estuaries, are of high interest in many parts of the world. Satellite data from both optical and radar sensors can help to monitor and investigate these changes. Data from both kinds of sensors being available for up to 30 years now, allow examinations over large timescales, while high resolution sensors developed within the last decade allow increased accuracy. So the creation of digital elevation models (DEMs) of, for example, the wadden sea from a series of satellite images is already possible. ENVISAT, successfully launched on March 1, 2002, continues the line of higher resolution synthetic aperture radar (SAR) imaging sensors with its ASAR instrument and now also allows several polarization modes for better separation of land and water areas. This article gives an overview of sensors and algorithms for waterline determination as well as several applications. Both optical and SAR images are considered. Applications include morphodynamic monitoring studies and DEM generation.

Keywords Waterline · Edge detection · Remote sensing · Morphodynamics · Digital elevation model (DEM) · Coastal area

1 Introduction

Two thirds of the world's population, some four billion people, live in coastal areas. In most cases, their lives depend on the morphological changes of the coast, the sediment transport of the ocean currents. Both erosion and deposition can be a problem: houses near cliffs may fall into the sea, growing river estuaries can cause flooding.

A. Niedermeier (✉) · D. Hoja · S. Lehner
Remote Sensing Technology Institute (MF),
German Aerospace Center (DLR), Wessling, German
E-mail: andreas.niedermeier@dlr.de

As an exemplar area, the tidal flats of the German Bight, especially the large river estuaries, are studied within this work. Methods are derived to monitor morphodynamics using satellite data from both synthetic aperture radar (SAR) and optical imaging sensors. Applications and possible new developments using ENVISAT and upcoming satellites are given.

The investigation area covers the German North Sea coast between the Netherlands and Denmark. Figure 1 gives an overview of this area. Examples given here cover the regions of the rivers 'Elbe' and 'Eider'. Additional studies on the river 'Weser' and the island 'Sylt' are mentioned.

The core of this article are methods to derive coastlines and waterlines[1] from satellite images of various types (Sect. 2). The waterlines can be used in many ways such as the generation of land/water masks, morphodynamic monitoring or the generation of digital elevation models (DEMs) (Sects. 3.1, 3.2, and 3.3 resp.). New developments and ideas for use with ENVISAT, upcoming satellites and enhanced sensor techniques like interferometric SAR are finally given in Sect. 4.

2 Waterline determination

In order to monitor morphodynamic changes of bottom topography, different methods for DEM generation have already been analyzed (Hoja 2000; Niedermeier et al. 2000; Wimmer et al. 2000). One approach is the so-called waterline extraction by image analysis.

Using extracted waterlines, several geoscientific applications can be carried out like identifying morphodynamic changes in bottom topography over a long time span and interpolation of waterlines from data acquired during a short time span into DEMs using

---

[1] A waterline is the instantaneous land–water boundary at the time of the imaging process. A coastline or shoreline is the waterline at the highest possible water level.
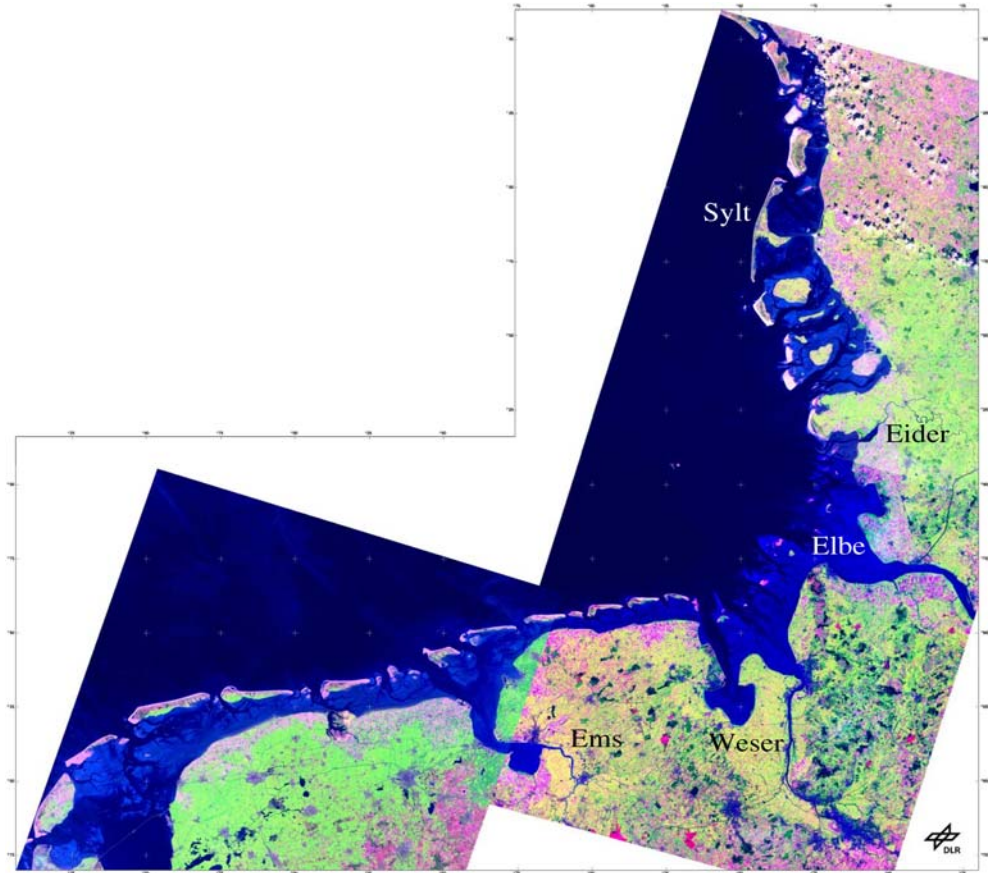
measurements from tide gauges as additional height information.

2.1 Extraction of waterlines from optical images

Different optical data sets have been used for waterline extraction so far. Table 1 gives an overview of different sensor systems with their geometric and spectral resolutions. Waterlines are extracted from optical remote sensing data using simple image processing techniques. Edge detection techniques are applied directly to the multi-spectral data set or on land/water masks received by classification. The true waterline position can be found best using a mid-infrared channel (Lee et al. 2001). For sensors without a mid-infrared channel, more sophisticated approaches are needed, e.g., a classification of image areas using a combination of other channels.

For the classification, a two-stage multi-spectral algorithm has proved to be valuable (Hoja 1999). First, a feature space analysis (Sabins 1987) is used to distinguish between water, tidal flats and land. Discrimination between tidal flats and land is possible due to the large amount of water in the tidal flats. In a second step, areas of interest are marked within the tidal flats as training areas, based on semi empirically determined spectral

signatures (Jensen 1995; Kraus and Schneider 1988). Finally a supervised classification with the maximum-likelihood operator is carried out. Resulting areas are divided into the super-classes 'flooded' and 'not flooded' and the boundary is extracted representing the actual water/land boundary at acquisition time.

Supervised classification of the tidal flats is based on prior knowledge about the sediments in the tidal flats and their typical spectral reflectance characteristics (Kraus and Schneider 1988; Lillesand et al. 2003). The result of classifying an IRS scene was verified at some points in the wadden sea during an expedition.

Table 1 Various optical sensors used for waterline determination

Satellite	Sensor	Geometric resolution (m)	Spectral bands
Landsat	MSS	80	2V + 2N + 1T
	ETM	30	3V + 1N + 2S + 1T
	PAN	5	1V
IRS	LISS-III	25	2V + 1N + 1S
SPOT	XS	10	2V + 1N + 1S
	PAN	5	1V
IKONOS	XS	4	3V + 1N
	PAN	1	1V
QUICKBIRD	XS	2.5	3V + 1N
	PAN	0.6	1V

Spectral bands: *V* visible; *N* near, *S* short wave, and *T* thermal infrared

Classification results showing the sediment distribution in the tidal flats is of high interest for administration and modellers. However, a thorough validation was not yet possible due to lack of in-situ data and the available geological maps being from the mid-seventies of the last century and, therefore, no longer valid in such morphodynamically active areas.

Another very common method for waterline extraction, which works effectively with all types of optical sensor is manual extraction based on visual interpretation. It is a very effective, straight-forward procedure, which is widely applied to remote sensing data. Although not a mathematical tool, the human eye, in general, is also able to detect edges and boundaries such as shorelines in satellite pictures. Additionally, rational judgement skills a profitable input in defining what is a relevant edge or what is not. There are limitations, of course. Besides, a certain monotony that may induce mistakes, manual digitizing throws up challenges regarding the resolution of the sensor. The second challenge refers to interpretation of a boundary, since mainly in the low-resolution images, colour shades may decay gradually.

Cloud-free optical scenes of a particular optical sensor are generally available only two to three times a year in temperate areas. Due to the resolution of the satellite data, features in the wadden sea up to about 100 m in size can be monitored now. Comparative studies of extracted topographic information using different sensors showed a very good overall agreement in spite of different sensor resolutions and algorithm accuracy (Rausch 2000; Zeug 2000).

2.2 Waterlines derived from SAR images

While useful optical images are only obtainable under good illumination and atmospheric conditions, synthetic aperture radar (SAR) also allows imaging of the Earth surface through clouds and at nighttime. Several SAR satellites are either in orbit now or will shortly be launched, Table 2 gives an overview.
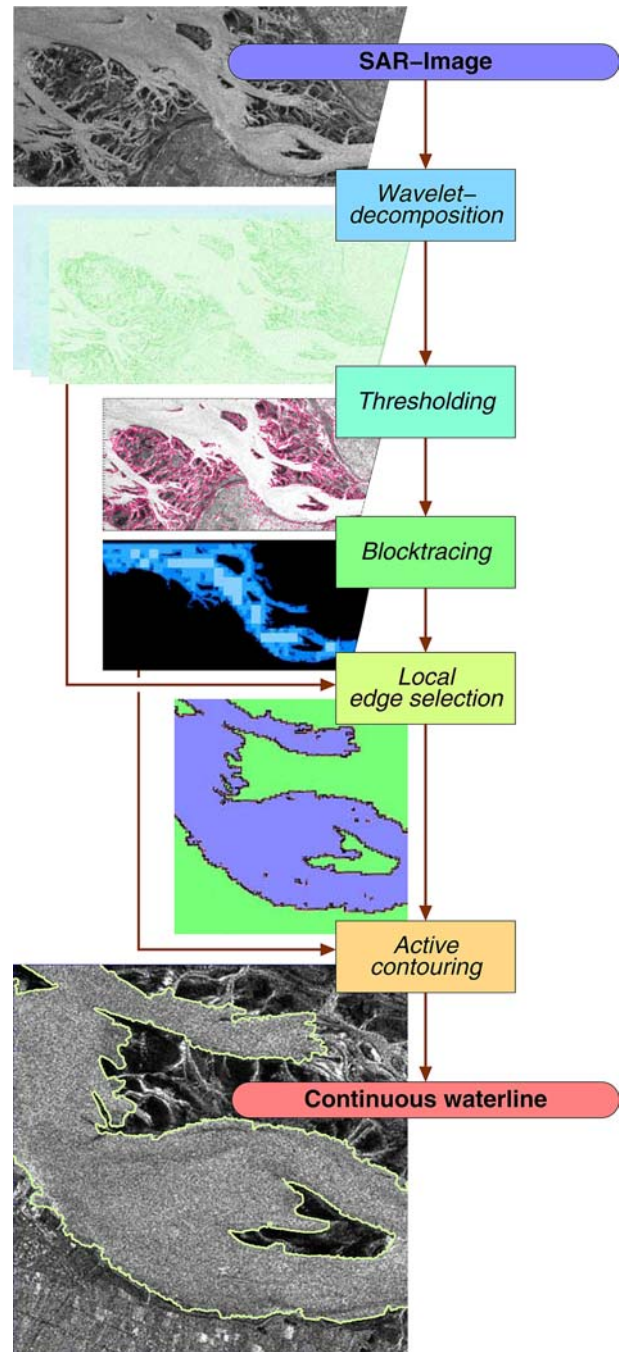
Due to its coherent illumination, SAR images, on the other hand are degraded by speckle, a multiplicative noise. This makes SAR image processing a far more challenging task, than the interpretation of images from optical sensors. Sophisticated and adapted algorithms

for SAR images are needed (e.g. (Dellepiane et al. 2004; Lee and Jurkevich 1990; Liu and Jezek 2004)).

An algorithm for waterline extraction from SAR images was developed (Niedermeier et al. 2000). It uses wavelet edge detection (decomposition and thresholding) as well as several post processing steps for the derivation of a continuous waterline from a single SAR image. Figure 2 gives an overview of the steps of this algorithm showing the intermediate results on an

Fig. 2 A wavelet based waterline extraction algorithm for SAR images

Table 2 Various SAR sensors used for waterline determination

Satellite (*planned* launch year)	Geometric resolution (m)	Polarizations
ERS-1/2 (1991/1995)	30	1
ENVISAT (2002)	30	2
RADARSAT-1 (1995)	9	1
RADARSAT-2 (*2005*)	3–10	4
COSMO-SKYMED (*2005*)	1–15	2
TerraSAR (*2006*)	1–6	4

exemplar SAR image from the estuary of the German river Elbe.

An amplitude density image (the point wise logarithm of a SAR amplitude image) is used as input to the wavelet edge detection method proposed by Mallat (Mallat and Hwang 1992; Mallat and Zhong 1992a). This method is based on a dyadic wavelet decomposition without subsampling followed by thresholding. It works as a sophisticated edge detection method on SAR images as investigated in (Niedermeier 2002). This edge detection method is used as a first step in the proposed waterline algorithm. The theory of the edge detection is based on a relation (Mallat and Hwang 1992) between the regularity of an image (which is different for 'homogeneous' speckle noise and image edges) and the decay of the wavelet coefficients along the scale a. The wavelet transform

$$\mathcal{W}_\psi I : (a, \mathbf{b}) \mapsto \frac{1}{|a|} \int_{\mathbb{R}^2} I(\mathbf{x}) \psi\left(\frac{\mathbf{x} - \mathbf{b}}{a}\right) \mathrm{d}^2\mathbf{x}, \tag{1}$$

of the image I is calculated for all image coordinates b on dyadic scales $a = 2^k$ using an iterative filter convolution (Mallat and Zhong 1992a) which is equivalent to integration with a spline wavelet ψ in (1).

Post-processing starts with an image segmentation into connected edge-free regions (water) and regions with higher edge density (land). The so-called block-tracing (Niedermeier et al. 2000) begins with large, edge free squares and attaches smaller ones recursively. Its result is a coarse image segmentation into water and land.

Within a small band of boundary between both regions, the strongest image edge is locally selected yielding edge fragments of the waterline. To connect these fragments to a continuous waterline, an active contour model (Mason and Davenport 1996; Williams and Shah 1992) is used. It minimizes certain energy integrals (representing length, curvature, area, etc.) iteratively along points of a closed curve $v : J \rightarrow \mathbb{R}, s \mapsto v(s)$. For each pixel of v, the energy function

$$E = \int_J \lambda_{\mathrm{con}} E_{\mathrm{con}}(s) + \lambda_{\mathrm{cur}} E_{\mathrm{cur}}(s) + \lambda_{\mathrm{img}} E_{\mathrm{img}}(s) \mathrm{d}s, \tag{2}$$

is calculated and minimized, where

$$E_{\mathrm{con}}(s) = \left|\frac{\mathrm{d}v}{\mathrm{d}s}(s)\right|^2, \tag{3}$$

and

$$E_{\mathrm{cur}}(s) = \left|\frac{\mathrm{d}^2 v}{\mathrm{d}s^2}(s)\right|^2, \tag{4}$$

are the internal energies (tension and curvature strength) of the curve v, $E_{\mathrm{img}}(s)$ is the external image energy, and $\lambda_k > 0$ are balancing parameters (Mason and Davenport 1996; Niedermeier et al. 2000).

Although some applications can handle waterline fragments, others (e.g. image segmentation) depend on a continuous waterline. Due to speckle artefacts or low image contrast, there are often a lot of small fragments which are joined by the active contour step.

The mean error of the location of the detected waterline was around 40 m in comparison to a model solution derived by visual inspection of an exemplar image of 1 million pixels (Niedermeier 2002). This is a very promising result taking into account that the ground resolution of ERS is around 30 m at a 12.5 m pixel spacing.

High resolution images from ERS/ENVISAT of an area are available 1–4 times a month. Automatic processing is possible on most of them while only a few bear disturbing features, e.g. due to very extreme weather situations. These can be corrected with a small manual interaction before the post-processing in roughly every second case.

2.3 Use of SAR coherence images

To overcome the problem of missing contrast of the land/water boundary in the SAR amplitude image, SAR coherency data was analysed. Use of interferometric coherence as a measure of the correlation of the scatterers between two SAR acquisitions serves as a criterion to distinguish between the land and sea surface.

For two complex SAR images c_1, c_2 of the same area, the coherence magnitude can be estimated in an Npoint neighbourhood of x_0 as

$$|\gamma| = \frac{\left|\sum_{j=0}^{N-1} c_1(x_j) c_2^*(x_j)\right|}{\sqrt{\sum_{j=0}^{N-1} |c_1(x_j)|^2 \sum_{j=0}^{N-1} |c_2(x_j)|^2}}, \tag{5}$$

where '*' denotes complex conjugation. $|\gamma|$ is a value in the interval [0, 1].

The coherency data used were derived from SAR images of the ERS satellites flown in tandem mode. In this mode, one acquisition per satellite is acquired of the same area only one day apart (multi-pass interferometry).

The algorithm to determine the coastline is purely based on an examination of the interferometric coherence (Schwäbisch et al. 1997). The extraction is performed in a first step with a series of basic image processing steps (filtering, gradient estimation) individually for each 'resolution level' (three have proved useful). These numbers of averaged samples are chosen within the preprocessing step of calculation of coherence. The second step in the coastline detection refines the individual lines again with basic image processing methods (opening, thinning). Finally, the individual lines are merged to yield an accurately positioned shoreline.

In contrast to waterline extraction from amplitude SAR data (as described in the previous section), this method is restricted to the detection of the line of highest

water level between the acquisitions. This is due to the fact that coherence maps describe the degree of stability of scatterers on a centimetre scale between two acquisitions. Areas having changed between the two acquisition dates due to being flooded therefore show different appearances in the two complex images which results in low coherence. Another drawback of the algorithm is the detection of areas in the tidal flats showing high coherence although they were flooded between the times of data acquisition.

Figure 3 shows part of the Elbe estuary with the coastline extracted from coherency data in red superimposed on the amplitude of the ERS-1 image. For comparison, the average high tide level was extracted from the conventional echo/sounder DEM and is also superimposed (in green) on the image. It can be seen that the coherency coastline is in good correspondence to the average high tide level in the south of the test site. The higher grade of detail in the line of highest water level provides additional knowledge. Variable high tide levels can result in bathymetric information. In the northeast corner, the extracted line seems to be shifted towards the water. The area between the red and green line are salt marshes in front of the dike, which were not flooded between the two data acquisitions and show high coherence. However, some areas within the shallows bordering the land are outlined by the algorithm as described in spite of being flooded between data acquisitions.

Closer investigation of these areas with high coherence in the Wadden sea showed that they are situated in higher regions, the dominating sediment is mud (smallest grain sizes), they are flooded only by currents of low velocity and the tidal flooding takes place only for a short time and at small water heights. Morphodynamic changes in this region are therefore only small and the area appears coherent in the images at both acquisitions (Hoja et al. 2002).

3 Applications

Waterline techniques introduced in the previous section were applied in various regions of the German Bight. In the following, we present waterline results and sketch their further use.

3.1 Use of land/water masks

The generation of a land/water mask using a waterline is relatively straightforward. Using preknowledge about certain points belonging to land or water, as e.g. given by the blocktracing segmentation in the SAR waterline algorithm, the regions on both sides of the waterline can easily be marked.

Waterlines from both optical and SAR images allow the generation of land/water masks (Fig. 4). Extracted from a single image they can be an input for other algorithms. Masking out the land area on SAR images is an important task when deriving wave parameters or wind fields. The knowledge of land areas can also help in automating the search for wind shadowing by land when resolving a 180° ambiguity in wind direction. Land usage classification on time series of SAR images as an agricultural application only makes sense in regions which are permanently unflooded.

Land/water masks are also important for optical images, e.g. ocean colour derivation yields bad results in shallow water areas, where instead of water constituents being sensed, the radiation traverses the waterbody and retrieves the sea floor.

Fig. 3 Coastline from ERS SAR coherence data in Elbe estuary, March 1996, superimposed on the ERS-1 amplitude image
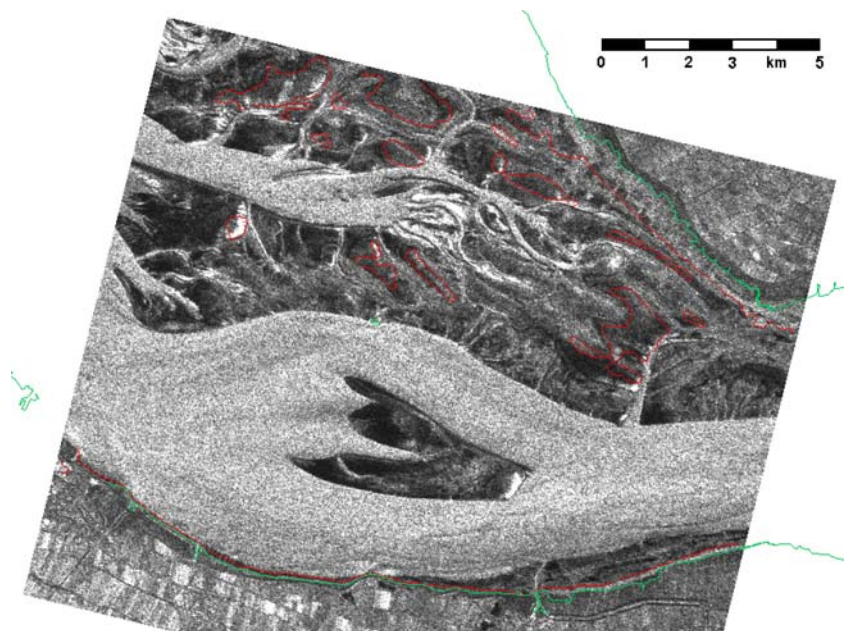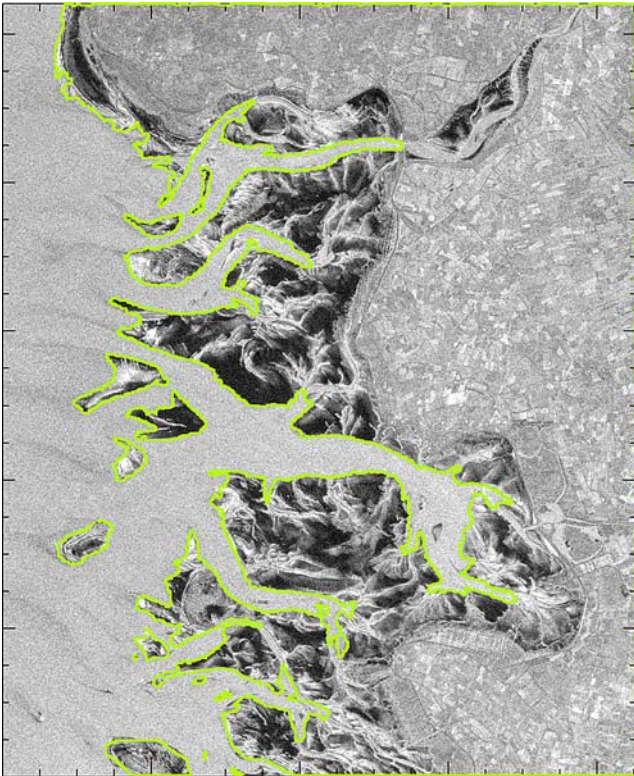
Fig. 4 Waterline in estuary of the German river Eider, SAR image from March 19, 1998

3.2 Monitoring the morphodynamics

With the tidal current moving the water several tens of kilometers twice a day, the sandbanks of the German Bight are subject to permanent change in both shape and position. A time series of satellite images of the same region in the wadden sea at a similar tidal phase allows the monitoring of the morphologically active areas. As an example, Fig. 5 shows the changes of a sandbank in the Eider estuary over a time span of 24 years. Waterlines were derived via visual interpretation using optical images. The dotted lines are less confident parts of the waterlines. Nevertheless, the results are remarkable: the centre of gravity of the sandbank shifts some 800 m (9 cm per day in average) while reducing in size and slightly rotating.

Within only 7 years (1992–1999), the south coast of the sandbank 'Medemsand' in the river Elbe estuary moved northwards some 850 m (corresponding almost 70 pixel in the geocoded ERS image). This was derived from three SAR images of this period, each at low tide situation (-1.8––-1.5 m absolute altitude according to nearby tide gauge values), as presented in Fig. 6. The automatic waterline detection mentioned in Sect. 2.2 was used here.

Using topographic information (either from echosounder measurements or interpolated as shown in the following section) the amount of transported sediment can be roughly estimated. According to the (vessel mounted) echosounder topography of 1996, provided by the German Federal Waterway Engineering and Research Institute (BAW), the river directly south of 'Medemsand' is some 20 m deeper than the sandbank which means about 2,400 m^3 (4,000 t) sand being transported per year per meter of coastline.

Data of the coastline of the German island Sylt included historic maps of the last two centuries, optical satellite images of the 1970s and 1980s and several SAR images from 1992 to 1998. Erosion on large parts of the island were stopped in the mid 20th century by human interaction. Nevertheless, the northern and southern tips are still changing their shapes. Details can be found in (Zeug 2000).

3.3 Generation of digital elevation models

For extraction of the bottom topography (to create an intertidal DEM), we consider a set of waterlines in a small region from satellite images taken during a small temporal interval, but covering many different water level situations. Usually this technique is applied to SAR images as the weather situation in the German Bight does not allow recording enough cloud-free optical images in a short time span. The interpolation of a DEM uses therefore the waterlines from these images as well as nearby (in space and time) information from a tidal gauge. Thereby the following simplifications are used:
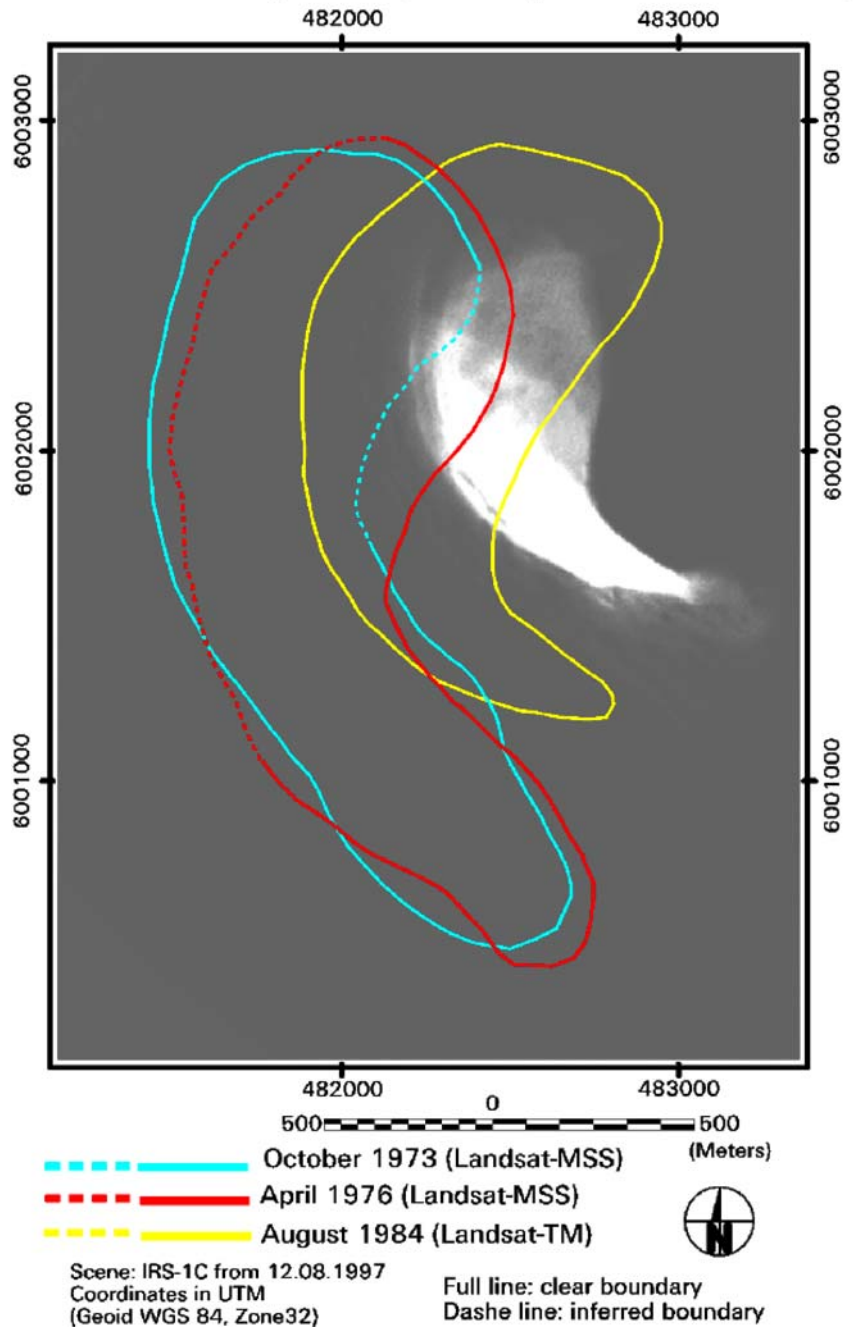
- The area is small enough to ignore the tidal slope of the water surface.
- The time period covering all images is short enough to ignore morphodynamical changes but long enough to have sufficiently many different tidal situations available.

Figure 7 presents 12 SAR images of the small sandbank 'Medemgrund' in the Elbe estuary, recorded between December 1996 and July 1998 in various tidal situations. Tidal heights taken from a tide gauge less than 10 km away from the sandbank were used to interpolate a topography by a Gaussian shaped interpolation weight function. The interpolation results are given in Fig. 8a. Regions outside the tidal height range of the 12 images allow no elevation extraction. A comparison with the same area from the vessel mounted echosounder topography from 1997 provided by BAW gave mean height differences of 30–40 cm (ignoring border effects from regions outside the tidal range considered, Fig. 8b gives the reference topography for values higher than -2.0 m NN).

DEMs like the one created, are important input for tidal modelling and its applications, e.g. flood prevention. By iterative methods, existing DEMs can also be modified using a single or very few waterlines and iterative runs of a tidal model (Mason et al. 1999). This is supposed to yield higher accuracies and larger regions being examined due to better tidal information about every point of the waterline as well as a shorter temporal

Fig. 5 Changes of the
sandbank 'Blauort' within two
decades using Landsat and IRS
images

Blauort shoal migration (over August 1997 IRS scene)

October 1973 (Landsat-MSS)
April 1976 (Landsat-MSS)
August 1984 (Landsat-TM)

Scene: IRS-1C from 12.08.1997
Coordinates in UTM
(Geoid WGS 84, Zone32)

Full line: clear boundary
Dashe line: inferred boundary

range of the images. Nevertheless a DEM and a tidal model are needed for the latter approach.

4 Conclusions and outlook

4.1 Waterline detection with ENVISAT

Besides the comparable SAR imaging modes from the ERS-1/2 satellites, which promise similar waterline quality, ENVISAT provides several new modes and sensors.

ScanSAR allows imaging of huge regions up to 500×500 km^2 in a single scene at a resolution of about 100 m. This reduces the quality of the derived waterline to a value of around 150–200 m meaning errors in the derived DEM of around 1 m as a rough estimation based on ERS results and coastal slopes. While a more frequent coverage would mean also easier coverage of the tidal range, reducing the morphological

Fig. 6 Changes of the sandbanks 'Medemsand' within 7 years using ERS-2 SAR images. Axes show pixel numbers (12.5 m pixel spacing)
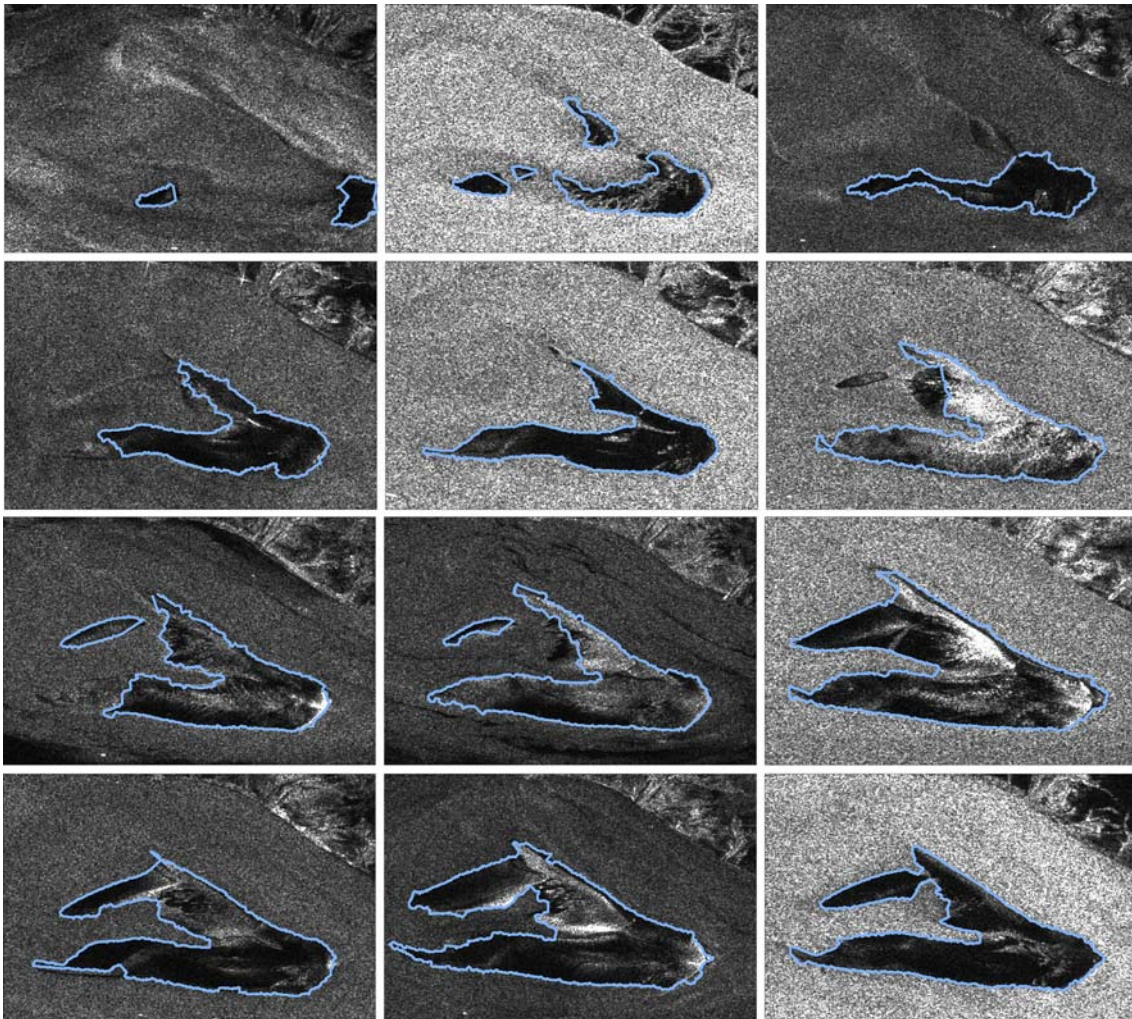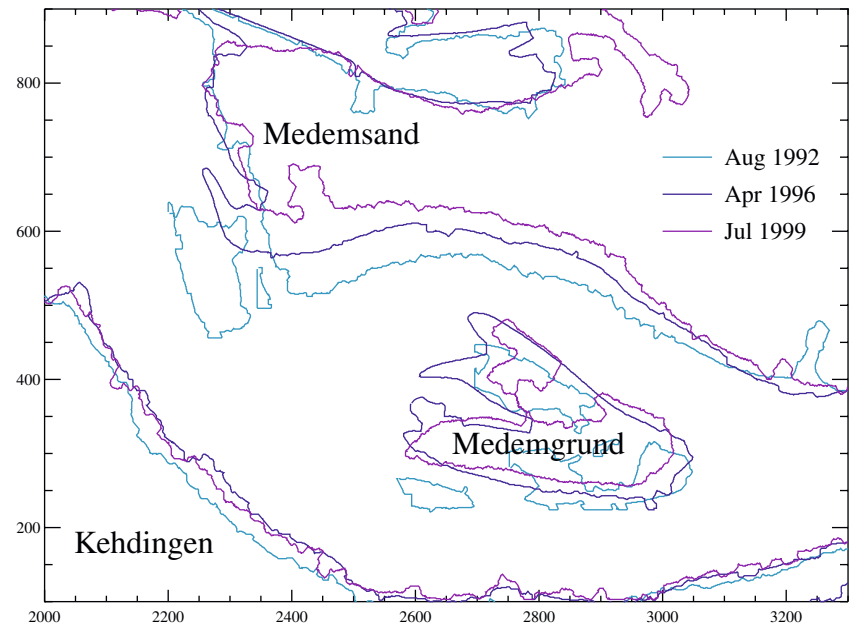
Fig. 7 Waterlines superimposed to SAR images of sandbank 'Medemgrund' in 12 cases during 1.5 years ordered by falling water level. The sandbank is totally covered by water almost half of the time
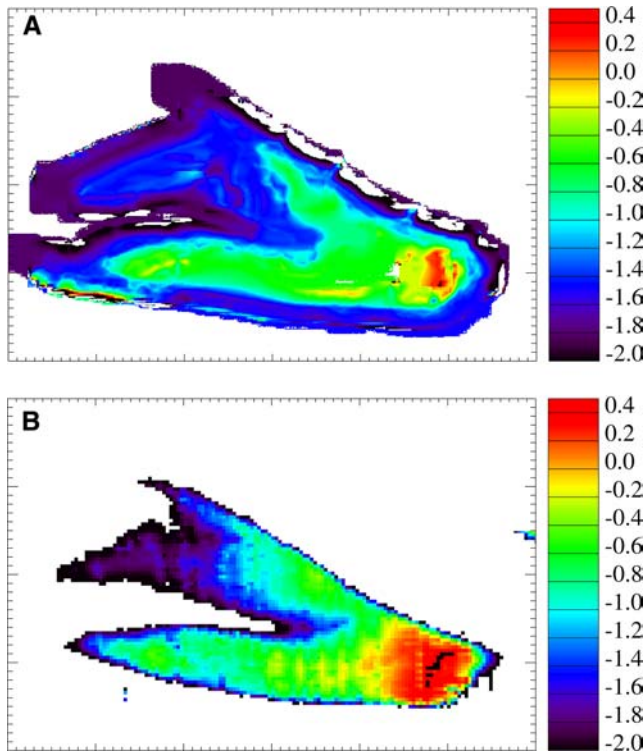
Fig. 8 Bottom topography (in meters) of the sandbank 'Medemgrund' interpolated from SAR images (**a**) in comparison to the echosounder based topography (**b**)

changes in the period under consideration, the error of the waterline localization will be the major contribution to the DEM error.

The optical sensor MEdium Resolution Imaging Spectrometer (MERIS) has 15 spectral bands at a resolution of 300 m. While being able to very confidently separate land and water areas with its relatively high spectral resolution, the spatial resolution is too low for waterline applications covered here. MERIS is a useful sensor for large scale applications like land/water mask generation for wind derivation.

4.2 Further sensors and methods

4.2.1 Upcoming satellites

Both recent and upcoming satellites provide much higher geometric resolutions, both in optical and SAR data. RADARSAT-2 e.g. will provide SAR images up to a resolution of 3 m, IKONOS and QUICKBIRD provide optical images of 1 m and 0.6 m resp., and Terra-SAR-X and COSMO-SKYMED will provide SAR images of 1 m resolution. Uses of these images will, by far, enhance the localization of the derived waterline and reduce the error of the interpolated bottom topography. The problems of automatic waterline extraction (Sect. 2) due to extreme weather situations in some SAR scenes might vary with the SAR look angle ϕ due to the radar

reflectivity σ_0 on the water being dependent on both wind speed and ϕ.

Using multipolarization SAR allows easier segmentation of different land coverage areas and thus more reliable waterline extraction using up to four possible polarization combinations. This will also enhance the quality of waterlines using multipolarized images from ENVISAT and COSMO-SKYMED (up to two polarizations per image), RADARSAT-2, and TerraSAR-X (both up to four polarizations per image).

4.2.2 DEMs from InSAR techniques

SAR interferometry (InSAR) is a technique by which elevation models are calculated using different running time between two acquisitions of the same area from slightly different positions of two antennas (Bamler and Hartl 1998; Siegmund et al. 2001). InSAR allows DEM generation of the wadden sea, if the cross-track baseline is suitable for the application. With this method, DEMs can only be generated of non-flooded areas. Therefore, the acquisition takes place during low tide situations.

Examination of data from the Shuttle Radar Topography Mission (SRTM, in February 2000) (Werner 2000) showed that the principal topographic shapes of the sandbanks in the Elbe estuary are visible (Niedermeier 2002; Voigt 2002), although the height accuracy (around 2 m, which is much better than the theoretically proposed 6 m) is still too low for the use in shipping or numerical tide modelling. Airborne InSAR allows an accuracy of a few centimeters at high spatial resolution (Wimmer et al. 2000) while its costs for mapping large regions are relatively high.

Also equipped with an InSAR mode, TerraSAR-X will not be able to measure topographies, as its baseline is proposed to be along-track only.

4.2.3 Other instruments

Some of the algorithms proposed in this paper are also applicable to aerial photography.

References

Bamler R, Hartl P (1998) Synthetic aperture radar interferometry. Inverse Probl 14:R1–R54

Dellepiane S, De Laurentiis R, Giordano F (2004) Coastline extraction from SAR images and a method for the evaluation of coastline precision. Pattern Recogn Lett 25:1461–1470

Hoja D (1999) Extraktion von Wasserstandslinien aus IRS-1C Szenen. Studienarbeit, Institut für Kartographie, Technische Universität Dresden, May 1999

Hoja D (2000) InSAR-Höhenmodell und Wasserstandslinienverfahren im Vergleich. Master's thesis, Institut für Kartographie, Technische Universität Dresden, January 2000

Hoja D, Lehner S, Schwäbisch M, Winkel N, Buchroithner MF (2002) Analysis of ERS tandem mode coherence maps in the german wadden sea. Int J Remote Sens (Submitted)

Jensen JR (1995) Introductory digital image processing: a remote sensing perspective, 2nd edn. Prentice Hall, Englewood Cliffs

Kraus K, Schneider W (1988) Fernerkundung, volume 1: Physikalische Grundlagen und Aufnahmetechniken. Ferd. Dümmlers Verlag, Bonn

Lee J-S, Jurkevich I (1990) Coastline detection and tracing in SAR images. IEEE T Geosci Remote Sens 28(4):662–668

Lee K-S, Kim T-H, Yun Y-S, Shin S-M (2001) Spectral characteristics of shallow turbid water near the shoreline on inter-tidal flat. Korean J Remote Sens 17(2):131–139

Lillesand TM, Kiefer RW, Chipman JW (2003) Remote sensing and image interpretation, 5th edn. Wiley, New York

Liu HX, Jezek KC (2004) A complete high-resolution coastline of antarctica extracted from orthorectified radarsat SAR imagery. Photo Eng Rem Sens 70(5):605–616

Mallat SG, Hwang WL (1992) Singularity detection and processing with wavelets. IEEE T Inform Theory 38(6):617–643

Mallat SG, Zhong S (1992a) Characterisation of signals from multiscale edges. IEEE T Pattern Anal Mach Intel 14(7): 710–732

Mason DC, Amin M, Davenport IJ, Flather RA, Robinson GJ, Smith JA (1999) Measurement of recent intertidal sediment transport in morecambe bay using the waterline method. Estuar Coast Shelf S 49:427–456

Mason DC, Davenport IJ (1996) Accurate and efficient determination of the shoreline in ERS-1 SAR images. IEEE T Geosci Remote Sens 34(5):1243–1253

Niedermeier A (2002) Wavelet-Methoden in der SAR-Bildverarbeitung—Ein Wavelet-basiertes Wasserstandslinienverfahren zur Topographiebestimmung im Wattenmeer. PhD thesis, Technische Universität München, 2002

Niedermeier A, Romaneeßen E, Lehner S (2000) Detection of coastlines in SAR images using wavelet methods. IEEE T Geosci Remote Sens 38(5):2270–2281

Rausch J (2000) Analysis of morphological changes in the Dithmarschen bight based on topographic, radar and optical data. Master's thesis, Institute of Geoscience, Christian Albrechts University Kiel, March 2000

Sabins FF Jr (1987) Remote sensing—principles and interpretation. Freemann, New York

Schwäbisch M, Lehner S, Winkel N (1997) Coastline extraction using ERS SAR interferometry. In: Proceedings of 3rd ERS Symposium on 'Space at the service of our Environment', Florenz, Italien, March 1997

Siegmund R, Bao M, Lehner S, Niedermeier A, Mayerle R (2001) Surface currents imaged with hybrid along and cross track interferometry. In: Proceedings of IGARSS'01 (Sydney, July 9th–14th 2001), IEEE 2001

Voigt Y (2002) Höhenmodelle und Strömungsmessungen im deutschen Wattenmeer aus SRTM-Daten. Master's thesis, Institut für Kartographie, Technische Universität Dresden, April 2002

Werner M (2000) Shuttle radar topography mission (SRTM)—mission overview. In: Proceedings of EUSAR2000, Munich, Germany, 2000

Williams DJ, Shah M (1992) A fast algorithm for active contours and curvature estimation. CVGIP: Imag Understan 55(1):14–26

Wimmer C, Siegmund R, Schwäbisch M, Moreira J (2000) Generation of high-precision DEMs of the wadden sea with airborne interferometric SAR. IEEE T Geosci Remote Sens 38

Zeug G (2000) Entwicklung und Veränderung der Westküste der Insel Sylt nach historischen Quellen und Satellitendaten. Master's thesis, Institut für Geographie, Ludwig-Maximilians-Universität München, February 2000